α-Cycloaltrin: Molecular Shape and Hydration Properties

Stefan Immel, Guido E. Schmitt, and Frieder W. Lichtenthaler

Institute of Organic Chemistry, Darmstadt University of Technology, Germany

Introduction

Solid-state structure

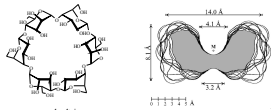

α-cycloaltrin
$^4C_1/^1C_4$ conformation (**1a**)

Cross section plot through the contact surface of **1a** and approximate molecular dimensions (2-OH/F3-OH side up).

The recent synthesis of α-cycloaltrin (α-CA, **1**) from α-cyclodextrin (α-CD)[1,2] opened up the possibility to analyze the conformational properties of this flexible cyclo-oligosaccharide in the solid-state and in solution, and to compare the results with those obtained from molecular modeling studies.

The very small energy difference for the $^4C_1$ and $^1C_4$ conformation of D-altropyranose (computed values vary from +0.8[3] to -1.5 kJ/mol[4]) leads to a unique solid-state structure of α-cycloaltrin (**1a**)[2], in which nearly perfect $^4C_1$ and $^1C_4$ chairs are arranged in an alternating sequence in a C_2 symmetrical conformation (left). Although this geometry lacks a "through-going" cavity, HTA calculations of α-cycloaltrin in vacuum[2,5] yield an *all*-skew (twist-boat) $^{1}S_{2}$-geometry (**1b**) as the global energy-minimum structure, which features a cavity (right picture). To get some insights into the conformation of α-cycloaltrin in aqueous solution, we performed molecular dynamics simulations and temperature dependent NMR studies[2,5,6].

HTA-simulation structure

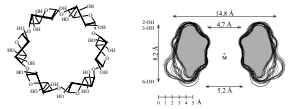

α-cycloaltrin
all-$^{1}S_{2}$ conformation (**1b**)

Cross section plot of a plane perpendicular to the macrocycle main plane with the contact surface of the α-CA **1b**.

NMR Analysis

High-resolution ^{1}H and ^{13}C NMR spectroscopy of **1** (D_2O, 30°C)[3] displays only one set of signals for the six altropyranoses, indicating that either fast conformational averaging between different pyranose ring forms takes place, or that in contrast to the solid-state a unique altrose geometry prevails in solution.

Table 1. Comparison of the altropyranoid ring ^{3}H-^{1}H-coupling constants calculated for the $^4C_1$, $^1C_4$, and *all*-$^{1}S_{2}$ (skew) forms of the α-cycloaltrin with those found (800 MHz[2], D_2O, 30°C)

coupling constants [Hz][a]	$^4C_1$	$^1C_4$	$^{1}S_{2}$ [b]	found	calc.[c]
$J_{1,2}$	2.2	8.0	4.0	4.73	4.9
$J_{2,3}$	2.7	10.2	10.2	8.19	8.3
$J_{3,4}$	3.4	2.4	4.5	3.71	3.5
$J_{4,5}$	9.7	1.4	6.4	5.32	5.5

[a] Calculation based on the Karplus-type H-C-C-H-torsion angle dependency of coupling constants, including the electronegativity effect of the substitution pattern by use of the generalized Haasnoot-equation[8]. [b] Data calculated of the HTA-derived global energy minimum *all*-skew form. [c] Least-squares fit for 26% $^4C_1$, 34% $^1C_4$, and 40% $^{1}S_{2}$.

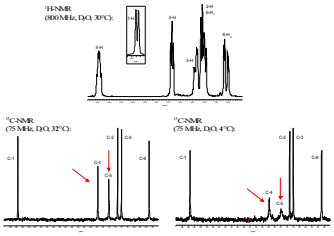

The ^{3}H-^{1}H coupling constants are consistent with either scenario: as indicated in Table 1, the experimental values agree with an average between the $^4C_1$ and $^1C_4$ forms (geometry **1a**), but correlate also surprisingly well with the values calculated for the *all*-$^{1}S_{2}$ form **1b**. The presence of conformational equilibria in aqueous solutions of **1** is indicated by the temperature dependency of its ^{1}H NMR data: the value of $J_{3,4}$ decreases from 8.2 Hz at 30°C to 7.6 and 7.1 Hz at 20 and 4°C, respectively, thereby narrowing the well separated signal for 3-H. Although the decreasing value of $J_{3,4}$ with decreasing temperature points towards the $^4C_1$ altrose conformation to be the most stable form in the $^4C_1 \rightleftharpoons {}^{1}S_{2} \rightleftharpoons {}^1C_4$ pyranose pseudorotational itinerary, as this form shows the lowest calculated coupling constant (cf.Table 1), the best fit of calculated vs. measured coupling constants was achieved for an approx. 1:1:1 mixture of $^4C_1$, $^{1}S_{2}$, and $^1C_4$ forms.

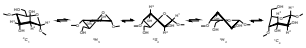

More profound effects are observed for the ^{13}C signals for C-4 and C-5, which are substantially broadened upon lowering the temperature from 30 to 4°C , providing further evidence for a dynamic equilibrium of various altrose geometries which starts to "freeze-out" at 4°C.

Molecular Dynamics Simulations

For both α-CA forms **1a** and **1b** MD simulations utilizing the CHARMM[9] force-field[10] with explicit incorporation of the (aqueous) solvent were performed (Fig.1). Although the macrocycles display a considerable degree of flexibility, no significant conformational transitions for the pyranose units were observed within a time frame of 600ps (Fig.2).

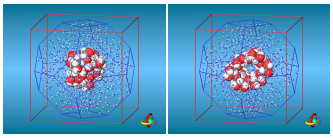

Fig. 1. MD simulation boxes of α-cycloaltrin **1** (left: **1a**, right: **1b**) surrounded by 606 and 611 water molecules, respectively (boxsize of the periodic truncated octahedron approx. 32 Å).

Obviously, any change of the pyranose conformations entails substantial rearrangements in the tightly bound first hydration shell, rendering these processes too slow to be observable during standard MD simulations. The MD trajectories were used to analyze the molecular parameters, conformations and hydration properties of both forms of α-CA **1a** and **1b**.

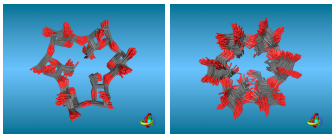

Fig. 2. Superimposition of 60 α-cycloaltrin (left: **1a**, right: **1b**) snapshot geometries taken in 10 ps intervals from 600 ps MD simulations in water (hydrogen atoms are omitted for clarity).

The plots on the right show the MD derived probability distributions of intersaccharidic and exocyclic torsions Φ (O_5-C_1-O_1-C_4), Ψ (C_1-O_1-C_4-C_3), and ω (O_5-C_5-C_6-O_6).

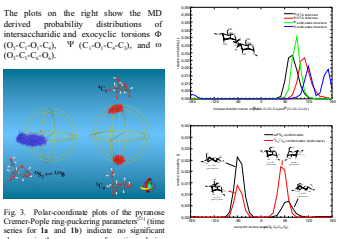

Fig. 3. Polar-coordinate plots of the pyranose Cremer-Pople ring-puckering parameters[11] (time series for **1a** and **1b**) indicate no significant changes in the pyranose conformations during the MDs.

Constrained MD Simulations

The effects on the macrocycle of changing one altrose unit in **1a** along the $^4C_1 \rightarrow {}^{1}S_{5} \rightarrow {}^1C_4$ pathway can be monitored within a reasonable nanosecond time frame by using constrained MD techniques: two pyranose ring torsion angles O_5-C_1-C_2-C_3 and C_2-C_3-C_4-O_4 of one altrose unit are restained in such a way, that the $^4C_1$ conformation is forced to vary in the desired direction (Fig.4, gray shaded altrose residue **B**). As this ring flip is artificially induced, the neighboring unconstrained monosaccharide units are subject to considerable intrinsic strain in the macro-ring: as one unit remains only slightly distorted towards $^4C_1 \rightarrow {}^{1}H_{2}$ (unit **A** in Fig.4), the second adjoining residue (**C**) displays a full transition along $^4C_1 \rightarrow {}^{1}S_{5} \rightleftharpoons {}^{2,5}B$. As this ring-flip was not induced by additionally applied MD potentials, it reveals the way conformational changes occur within α-CA (**1**). Flexure of the altrose chair geometries must involve $^{1}S_{5}$ forms, cooperatively affecting neighboring units to also flip into this intermediate as these are tied up in a macrocyclic "strait-jacket". The consecutive "rolling around" of geometry changes in the conceivably elliptically distorted macrocycle leads to a statistical scrambling of $^4C_1$, $^1C_4$, and $^{1}S_{5}$ forms in **1** in aqueous solution, and the NMR data provide an averaged picture thereof. As the two forms **1a** and **1b** are to be considered as the limiting structures of a complex equilibrium only, the inclusion complex formation capabilities of α-CA (**1**) must be closely correlated to its solution conformations, of which only the all-$^{1}S_{2}$ form **1a** features a sizable "through-going" cavity with which to incorporate potential guest molecules.

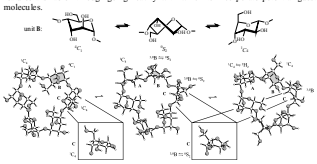

Fig. 4. Constrained MD simulations of α-CA display a conformational transition of the central $^4C_1$ altropyranose (gray shaded unit **B**) of a 'C_2-C_3-C_4-O_4'-fragment (units **A**-**B**-**C**) in the macrocycle.

Hydration Properties, Water Densities, and Solvent Structuring

Table 2. Summary of the hydration properties for the conformations **1a** and **1b** of $^4C_1$-α-CA as derived from the MD simulations in aqueous solution.

hydration properties	solid-state conformation (**1a**)	*all*-$^{1}S_{2}$ conformation (**1b**)
number of water molecules		
first hydration sphere	102 - 112	104 - 113
hydrogen-bonded in the cavity	30.6 ± 2.8 2.0 ± 0.2 [a]	39.6 ± 3.4 5.3 ± 0.9
intramolecular H-bonds	6.1 ± 1.6	3.1 ± 1.4
intermolecular H-bonds		
total solute-solvent	35.9 ± 3.2 [b]	45.0 ± 3.7
solute-O - H-OH	24.6 ± 2.4	27.6 ± 3.5
solute-O-H - OH$_2$	11.3 ± 1.8	17.4 ± 1.0

[a] see "through-going" cavity, but surface indentation only.
[b] smaller differ from number of hydrogen-bonded water molecules due to water bridges solute-OH - OH$_2$ - O-solute.

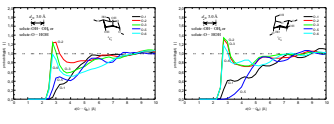

Fig. 5. The above plots give the MD derived radial pair distribution functions[2,3] of water oxygen atoms around the α-CA solute oxygens, i.e. the spherically averaged probability to find a water molecule around the hydroxyl groups and acetal oxygens (upper right plot: averaged probability for the $^4C_1$ units of **1b**; lower plots: pair distributions for the $^4C_1$ and $^1C_4$ units of **1a**, respectively). The sharp peaks at around 3.0 Å (hydrogen-bonding distance between solute and solvent) indicate a well defined first hydration shell around the 2-, 3-, and 6-OH groups, whereas the O-1 and O-5 oxygen atoms are less hydrated. Small fluctuations of the pair distribution functions at larger distances (4.5-6.0 Å) indicate a weak second hydration sphere; at distances >6.0 Å the relative water densities reach the standard value of 1.0 for the bulk phase.

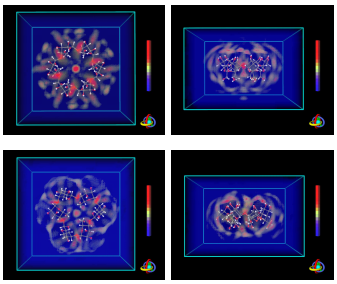

Fig. 6. Front- (left) and side-views (right) of the three-dimensional water probability densities around α-CA (top pictures: conformation **1b**, bottom: **1a**); opaque red to orange-yellow colors indicate increased water densities around the solute in relation to the bulk phase water (transparent blue colors). The contours were obtained from 3D-fitting and superimposition of all MD snapshot geometries of α-CA (incl. solvent; **1a**: 11440 configurations, **1b**: 12562), and counting the relative water densities on an orthogonal grid (bulk water density = 1.0). The orange-red spatial regions correlate with the well-defined first hydration shell of α-CA around the 2-, 3-, and 6-OH groups (compare to Fig. 5). For both **1a** and **1b**, the center red spots correspond to trapped water molecules of decreased mobility inside the cavity (**1b**) or the surface indentation (**1a**) of α-CA.

References

[1] Y. Nogami, K. Fujita, K. Ohta, K. Nasu, H. Shimada, C. Shinohara, and T. Kogz. A new synthetic strategy of cyclooligosaccharides: cyclodextrin-derived cycloaltrins made up from α(1→4)-linked altropyranoses. *J. Inclusion Phenom. Mol. Recognit. Chem.* **1996**, *25*, 57-60.

[2] Y. Nogami, K. Nasu, T. Koga, K. Ohta, K. Fujita, S. Immel, H.J. Lindner, G.E. Schmitt, and F.W. Lichtenthaler: Synthesis, structure, and conformational features of α-cycloaltrin: a cyclo-oligosaccharide with alternating $^4C_1/^1C_4$ pyranoid chairs. *Angew. Chem.* **1997**, *109*, 1987-1991; *Angew. Chem. Int. Ed. Engl.* **1997**, *36*, 1899-1902.

[3] S.J. Angyal: The conformations and ratios of aldopyranoses in aqueous solution. *Aust. J. Chem.* **1968**, *21* ,2737-2746.

[4] M.K. Dowd, A.D. French, and P.J. Reilly: Modeling of aldopyranosyl ring puckering with MM3 *Carbohydr. Res.* **1994**, *264*, 1-19.

[5] F.W. Lichtenthaler and S. Immel, The lipophilicity patterns of cyclodextrins and non-glucose cyclooligosaccharides. *J. Inclusion Phenom. Mol. Recognit. Chem.* **1996**, *25*, 3-16.

[6] The 3D-structures can be viewed at
"http://caramel.oc.chemie.tu-darmstadt.de/immel/3Dstructures.html",
MOLCAD graphics are available at
"http://caramel.oc.chemie.tu-darmstadt.de/immel/molcad/Gallery.html"

[7] We are most grateful to Prof. Dr. C. Griesinger and Dr. H. Schwalbe, for kindly determining the 800 (1H) and 200 (^{13}C) MHz NMR data at the 'Large Scale Facility for Biomolecular NMR' of Frankfurt University.

[8] C.A.G. Haasnoot, F.A.A.M. De Leeuw, and C. Altona: The relationship between proton-proton NMR coupling constants and substituent electronegativities. *Tetrahedron* **1980**, *36*, 2783-2792.

[9] B.R. Brooks, R.E. Bruccoleri, B.D. Olafson, D.J. States, S. Swaminathan, and M. Karplus: CHARMM: a program for macromolecular energy, minimization, and dynamics. *J. Comp. Chem.* **1983**, *4*, 187-217.

[10] S. Reiling, M. Schlenkrich, and J. Brickmann: Force-field parameters for carbohydrates, *J. Comp. Chem.* **1996**, *17*, 450-468.

[11] D. Cremer and J.A. Pople: A general definition of ring puckering coordinates. *J. Am. Chem. Soc.* **1975**, *97*, 1354-1358.

[12] M.P . Allen and D.J. Tildesley, Computer Simulation of Liquids, **1996**, Clarendon Press, Oxford.

[2] Lichtenthaler, F.W., and Immel, S. (1994). Cyclodextrins, cyclomannins, and cycloalactins with five and six (1®4)-linked sugar units: a comparative assessment of their conformations and hydrophilicity potential profiles. Tetrahedron: Asymmetry, 5, 2045-2060. - Lichtenthaler, F.W., and Immel, S. (1996). The lipophilicity patterns of cyclodextrins and non-glucose cyclooligosaccharides. J. Inclusion Phenom. Mol. Recognit. Chem., 25, 3-16.

[6] Lindner, H.J., and Kroeker, M. (1997). PIMM91 - *Closed Shell PI-SCF-LCAO-MO-Molecular Mechanics Program*, Darmstadt University of Technology.- Smith, A.E., and Lindner, H.J. (1991). π-SCF-Molecular Mechanics PIMM: formulation, parameters, applications. *J. Comput. Aided Mol. Des.* 5, 235-262.